

---

# Long-range Electron Transfer in Biology

Jay R. Winkler

California Institute of Technology, Pasadena, CA, USA

---

1	Introduction	1
2	Electron-transfer Theory	1
3	Chemically Modified Proteins	3
4	Protein–Protein Reactions	6
5	Photosynthesis and Respiration	8
6	Concluding Remarks	10
7	Related Articles	10
8	References	10

---

## 1 INTRODUCTION

Electron-transfer (ET) reactions, the simplest chemical transformations, play vital roles in a diverse ensemble of biological processes. Biological electron transfer is an extraordinarily vibrant field of inquiry, responsible for thousands of original research articles during the past decade. This chapter will focus on studies of ET in chemically modified proteins, protein–protein complexes, and two key biological energy transduction pathways, photosynthesis (*see Photosynthesis*) and respiration (*see Cytochrome Oxidase*).

Aerobic organisms derive most of the energy needed for life processes by the burning of foodstuffs with molecular oxygen in air.<sup>1</sup> In the first part of the respiratory process, hydrogen atoms are extracted from organic molecules. The hydrogen carriers provide reducing equivalents to the respiratory chain located in cell organelles (mitochondria) or, in bacteria, in the cell membrane. These chains consist of a series of membrane-bound protein complexes in which the hydrogen atoms are split into protons and electrons. The electrons are passed down the chain and reduce molecular oxygen to water, whereas protons are left behind on one specific side of the membrane. In addition, the electron current through the chain is coupled to the pumping of additional protons from water to the same side of the membrane.<sup>2</sup> The two proton currents lead to an increased positive charge and decreased pH on this side. The resulting electrochemical potential across the membrane drives the synthesis of ATP, the universal energy currency of living cells.

Photosynthesis is the natural complement to respiration. Photons from the sun induce charge separation in a membrane-bound redox chain, ultimately producing a transmembrane potential for ATP synthesis. In green plants, algae, and

cyanobacteria, the photogenerated holes oxidize water to oxygen. The photochemically generated reducing equivalents produce NADPH that, along with ATP, is used in carbon dioxide fixation.

Highly optimized ET reactions are essential for the operation of these biochemical machines. Much of the research on biological electron transfer aims to define the electronic and structural factors that regulate the rates and efficiencies of these essential transformations. This chapter will focus on studies of ET through proteins, particularly metalloproteins. ET processes involving DNA molecules have been the subject of extensive research as well,<sup>3–6</sup> but this work is beyond the scope of this chapter.

## 2 ELECTRON-TRANSFER THEORY

The unique simplicity of ET reactions has fostered the development of a powerful theoretical formalism that describes the rates of these processes in terms of a small number of parameters.<sup>7</sup> The conceptual breakthrough that led to the development of ET theory involved the recognition of the pivotal role played by the Franck–Condon principle.<sup>8,9</sup> Owing to the much higher electron velocities, nuclei remain fixed during the actual electron transfer from donor to acceptor. The transition state for this reaction must lie at a point in nuclear-configuration space where the reactant and product states are degenerate (Figure 1). Hence, through fluctuations of the reacting molecules and their surroundings, the transition-state configuration will be reached and an electron can transfer.

### 2.1 Activation Barriers

According to classical (Marcus) theory, the activation barrier for an adiabatic ET reaction depends on two parameters, the driving force ( $-\Delta G^\circ$ ) and the reorganization energy ( $\lambda$ ).<sup>7</sup> The reorganization parameter reflects the extent of outer-sphere ( $\lambda_{\text{OUT}}$ ) and inner-sphere ( $\lambda_{\text{IN}}$ ) nuclear rearrangement that accompanies charge transfer. The  $\lambda$  values for a cross reaction between two different reagents can be estimated from the average of the electron self-exchange reorganization energies for each redox partner (i.e.  $\lambda_{12} \approx \lambda_{11}/2 + \lambda_{22}/2$ ). The unique prediction from Marcus theory is that rates reach a maximum when the driving force equals the reorganization energy. At higher driving forces, rates are predicted to decline (inverted effect) owing to less favorable Franck–Condon factors for the electron transfer. The central lesson of classical theory is that nuclear rearrangements accompanying ET must be compensated by reaction driving force (Figure 1). The balance between  $\Delta G^\circ$  and  $\lambda$  is a direct consequence of protein structure.

Electron transfer in proteins generally involves redox centers separated by long distances. The electronic interaction

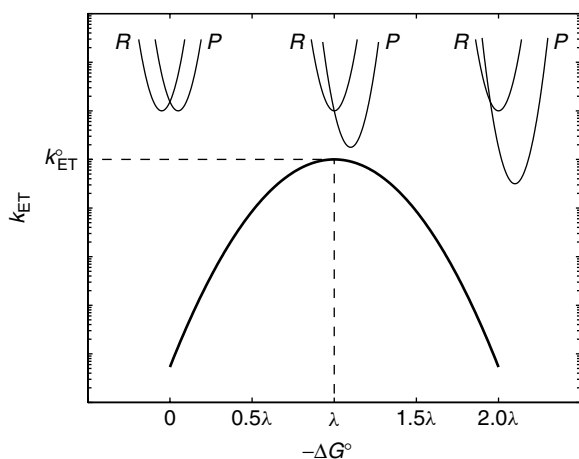


**Figure 1** Driving-force dependence of ET rates predicted by semiclassical theory (equation 1). Rates increase with driving force until they reach a maximum value ( $k_{ET}^0$ ) at  $-\Delta G^\circ = \lambda$ . Rates then decrease at higher driving forces (inverted effect)

between redox sites is relatively weak and the transition state for the ET reaction must be formed many times before there is a successful conversion from reactants to products; the process is electronically nonadiabatic. A Landau–Zener treatment of the reactant–product transition probability produces the familiar semiclassical expression for the rate of nonadiabatic electron transfer between a donor (**D**) and acceptor (**A**) held at fixed distance (equation 1).<sup>7</sup> Biological electron flow over long distances with a relatively small release of free energy is possible because the protein fold creates a suitable balance between  $\Delta G^\circ$  and  $\lambda$  as well as adequate electronic coupling between distant redox centers.

$$k_{ET} = \sqrt{\frac{4\pi^3}{h^2\lambda RT}} H_{AB}^2 \exp\left\{-\frac{(\Delta G^\circ + \lambda)^2}{4\lambda RT}\right\} \quad (1)$$

### 2.1.1 Redox Potentials

The reduction potentials of redox-active proteins are exquisitely sensitive to the structure of the polypeptide.<sup>10–13</sup> It is well known that homologous proteins from different organisms can have quite disparate amino acid sequences yet nearly identical three-dimensional structures.<sup>14,15</sup> Nevertheless, single-point mutations can destroy redox function without disrupting structure. Indeed, substitution of a single amino acid in myoglobin can shift the Fe(III/II) reduction potential by as much as 200 mV, effecting greater than a thousand-fold change in the equilibrium constant for reaction with a redox partner.<sup>16</sup>

The secondary and tertiary structures of a protein can modulate the reduction potential of a single cofactor by more than 500 mV. The Fe(III/II) reduction potential of a free heme in aqueous solution is approximately  $-200$  mV versus the normal hydrogen electrode (NHE), the potential of

cytochrome *c* is 260 mV, and that of cytochrome *f* reaches 450 mV.<sup>17</sup> The shift in reduction potential is reflected in a differential folding free energy of the oxidized and reduced proteins.<sup>18</sup> In the case of cytochrome *f*, the Fe(II) protein is more stable toward unfolding than the oxidized protein;<sup>19</sup> the redox potential indicates a stability differential of some 650 meV ( $63 \text{ kJ mol}^{-1}$ ). In order for cytochrome *f* to be a viable redox protein, the folding free energy of the oxidized form must be at least  $2 k_B T$  ( $\sim 5 \text{ kJ mol}^{-1}$  at 298 K), requiring that the folding free energy of the reduced protein be greater than  $68 \text{ kJ mol}^{-1}$  (700 meV).

### 2.1.2 Reorganization Energy

The protein fold plays a central role in lowering the reorganization energy of a biological ET reaction.<sup>10</sup> A large part of the  $\lambda$ -reduction results from sequestering a redox center from the aqueous solvent environment. Continuum models suggest that embedding a redox center inside a low dielectric cavity can lower the outer-sphere reorganization energy by as much as 50%.<sup>20</sup> Moreover, by constraining the coordination environment around metal centers, inner-sphere reorganization energy can be reduced as well.<sup>10</sup> Indeed, metals that are typically poor redox reagents because of large reorganization barriers can be extremely efficient when embedded in protein interiors. The reorganization energy for electron self-exchange in  $\text{Cu}(\text{phen})_2^{2+/+}$ , for example, is  $\sim 2.4 \text{ eV}$ ; the value for Cu(II/I) in *Pseudomonas aeruginosa* azurin is 0.7 eV. The 1.7-eV reduction in  $\lambda$  reflects the transition-state stabilization imposed by the azurin fold.<sup>10,21</sup>

It is important to remember that the reorganization energy is a composite parameter rather than a fundamental physical quantity. Refinements to the semiclassical theory usually arise from quantum mechanical treatments of vibrational motions.<sup>22</sup> The increased rigor associated with these models, however, is rarely accompanied by the extra data required to cope with the influx of new parameters. The approximations involved in its definition, and the errors associated with its measurement dictate that  $\lambda$  should never be expressed with great precision.

## 2.2 Electronic Coupling

The ability to control redox potentials and reorganization energies in proteins comes at a price: ET partners buried within insulating polypeptides cannot come into close contact to exchange electrons. The essential electronic interaction between redox cofactors must be mediated by the polypeptide matrix. Extensive experimental and theoretical efforts have been aimed at elucidating the factors that regulate distant electronic couplings between redox sites in proteins.<sup>21,23,24</sup>

The electronic coupling matrix element ( $H_{AB}$ ) reflects the strength of the interaction between reactants and products at the nuclear configuration of the transition state. Square-barrier ET tunneling models predict that the coupling will

depend exponentially on the distance ( $r$ ) between redox centers (equation 2).<sup>25</sup> A square tunneling barrier implies that a homogeneous medium separates the donor and acceptor. This model is appropriate for electron tunneling across a vacuum ( $\beta = 3-5 \text{ \AA}^{-1}$ ) and is a reasonable

$$H_{AB}(r) = H_{AB}(r_o) \exp \left\{ -\frac{1}{2} \beta (r - r_o) \right\} \quad (2)$$

approximation for tunneling through glassy solvents ( $\text{H}_2\text{O}$ ,  $\beta = 1.65 \text{ \AA}^{-1}$ ;<sup>26</sup> 2-methyltetrahydrofuran,  $\beta = 1.2 \text{ \AA}^{-1}$ ).<sup>27</sup> Superexchange models are better suited to the description of tunneling through inhomogeneous media. In 1961, McConnell described a superexchange model for electron tunneling from a donor to an acceptor across a bridge composed of  $n$  identical repeat units.<sup>28</sup> The electronic coupling matrix element is a function of the couplings between redox sites and the bridge ( $h_{Ab}$ ,  $h_{bB}$ ), the coupling between bridge elements ( $h_{bb}$ ), and the gap ( $\Delta\varepsilon$ ) between the energy of tunneling electron (or hole) and reduced (or oxidized) bridge states (equation 3).

$$H_{AB} = \frac{h_{Ab}}{\Delta\varepsilon} \left( \frac{h_{bb}}{\Delta\varepsilon} \right)^{n-1} h_{bB} \quad (3)$$

The medium separating redox sites in proteins is comprised of a complex array of bonded and nonbonded contacts and an *ab initio* calculation of coupling strengths is a formidable challenge.<sup>29</sup> The homologous-bridge superexchange model (equation 3) is not suitable because of the diverse interactions in proteins. Beratan and Onuchic developed a generalization of the McConnell superexchange coupling model that accommodates the structural complexity of a protein matrix.<sup>30</sup> In this tunneling-pathway model, the medium between **D** and **A** is decomposed into smaller subunits linked by covalent bonds, hydrogen bonds, or through-space jumps. Each link is assigned a coupling decay ( $\varepsilon_C$ ,  $\varepsilon_H$ ,  $\varepsilon_S$ ), and a structure-dependent searching algorithm is used to identify the optimum coupling pathway between the two redox sites. The total coupling of a single pathway is given as a repeated product of the couplings for the individual links (equation 4). The variation of ET rates with  $r$  depends upon the coupling-decay factors

$$H_{AB} = \Pi \varepsilon_C \Pi \varepsilon_H \Pi \varepsilon_S \quad (4)$$

for hydrogen bonds ( $\varepsilon_H$ ), van der Waals contacts ( $\varepsilon_S$ ), and single covalent bonds ( $\varepsilon_C$ ). Equation (3) suggests that the magnitude of  $\varepsilon_C$  should depend critically upon the energy of the tunneling electron relative to the energies of the bridge hole and electron states. Clear demonstrations of this energy dependence in the tunneling regime have been elusive. Studies, however, have shown that electron transport over exceptionally long distances is possible when hole or electron states of the bridge can be populated as real intermediates.<sup>31,32</sup> In comparing ET data from different protein systems, then, it is important to consider the tunneling-energy gap and the

possibility of forming oxidized or reduced intermediates in the bridging medium.

The tunneling-pathway model has proven to be one of the most useful methods for estimating distant electronic couplings.<sup>21,23,30,33</sup> The original tunneling-pathway model successfully described the distance dependence of protein ET reactions when a single pathway dominated the coupling.<sup>30</sup> The model was less successful when multiple pathways contributed to the overall coupling. More elaborate computational protocols have since been developed to describe in greater detail the factors that determine distant couplings in proteins.<sup>29,33-38</sup>

### 3 CHEMICALLY MODIFIED PROTEINS

#### 3.1 Ru-modified Proteins

Semiclassical theory provides a framework for understanding biological electron flow; what is necessary on the experimental front are systematic investigations of the response of rates to variations in ET parameters ( $\Delta G^\circ$ ,  $\lambda$ ,  $r$ ). Early efforts involving studies of bimolecular ET reactions were frustrated by the effects of diffusion. A simple bimolecular ET reaction can be broken into a sequence of three steps: diffusive formation of an encounter or precursor complex (**DA**); ET from donor to acceptor within the precursor complex (**DA**  $\rightarrow$  **D<sup>+</sup>A<sup>-</sup>**); and dissociation of the successor

$$k_{\text{obs}} = \frac{k_{+\text{D}} k_{\text{ET}}}{k_{-\text{D}} + k_{\text{ET}}} \quad (5)$$

complex to give products. The precursor and successor complexes are rarely observed in ET reactions; it is reasonable to employ a steady-state approximation to describe the time dependence of the [**DA**] concentration (i.e.  $\partial[\text{DA}]/\partial t = 0$ ). Within the limits of this approximation, the observed second-order rate constant for a bimolecular ET reaction (equation 5) depends on the rates of formation and dissociation of the precursor complex ( $k_{+\text{D}}$  and  $k_{-\text{D}}$ , respectively) and the ET rate within the complex ( $k_{\text{ET}}$ , equation 1). Below the diffusion limit (i.e.  $k_{\text{ET}} \ll k_{-\text{D}}$ ),  $k_{\text{obs}}$  is equal to  $K_{[\text{DA}]} k_{\text{ET}}$  (where  $K_{[\text{DA}]} = k_{+\text{D}}/k_{-\text{D}}$  is the equilibrium constant for precursor-complex formation). Since the value of  $K_{[\text{DA}]}$  is usually not known, it is quite difficult to extract accurate values of  $\lambda$  and  $H_{AB}$  from low-driving-force bimolecular ET rates. At high driving forces, reaction rates become masked by diffusion (i.e.  $k_{\text{ET}} \gg k_{-\text{D}}$ ,  $k_{\text{obs}} = k_{+\text{D}}$ ), frustrating efforts to observe inverted driving-force behavior.

In order to circumvent these difficulties, experimentalists developed methods to study the rates of intraprotein ET reactions.<sup>21,23,24,39</sup> One early approach involved metalloproteins that had been surface-labeled with redox-active metal complexes.<sup>40,41</sup>

### 3.2 Reorganization Energy

#### 3.2.1 Cytochrome *c*

Investigations of intramolecular ET in heme proteins have focused on cytochrome *c* (104 amino acids in the horse protein; 12.5 kDa;  $E^\circ = 0.26$  V vs. NHE) (see **Iron: Heme Proteins & Electron Transport**) (Figure 2).<sup>14,15</sup> Early work with the Ru–ammine modified protein involved the replacement of the native Fe center with Zn. Long-range ET reactions were initiated by visible-light excitation of the resulting Zn-porphyrin (ZnPor) to its long-lived (>10 ms), strongly reducing ( $E^\circ \sim -0.8$  V vs. NHE) triplet-excited state. A driving-force study of ET rates in Ru(NH<sub>3</sub>)<sub>4</sub>L(His33)-modified Zn-substituted cytochrome *c* (L = NH<sub>3</sub>, pyridine, isonicotinamide) was consistent with  $\lambda_{12} = 1.2$  eV.<sup>23,42</sup> The self-exchange reorganization energies for Ru-ammine complexes ( $\lambda_{11}$ ) are in the vicinity of 1.6 eV. Intramolecular ET kinetics, then, suggest that  $\lambda_{22} = 0.8$  eV for Zn-cytochrome *c*.<sup>42</sup>

Studies of high-driving-force ET in heme and nonheme proteins were made possible by Ru-diimine labeling protocols and the ‘flash-quench’ triggering method.<sup>43</sup> The driving-force dependence of ET in Ru(diimine)<sub>2</sub>(im)(His33)-modified Fe-cytochrome *c* (im = imidazole) is best described by  $\lambda_{12} = 0.8$  eV.<sup>21,23</sup> This value is lower than that found for Ru-ammine-modified Zn-cytochrome *c* because the diimine ligands coordinated to the Ru center are larger and more hydrophobic than ammines. Consequently, the self-exchange reorganization energy for Ru(diimine)<sub>2</sub>(im)(His)<sup>3+/2+</sup> is substantially smaller ( $\lambda_{11} = 0.8$  eV) than that of the ammine.<sup>23,42</sup> The combined results from ET measurements in the Ru–ammine and Ru–diimine proteins suggest that the reorganization energy

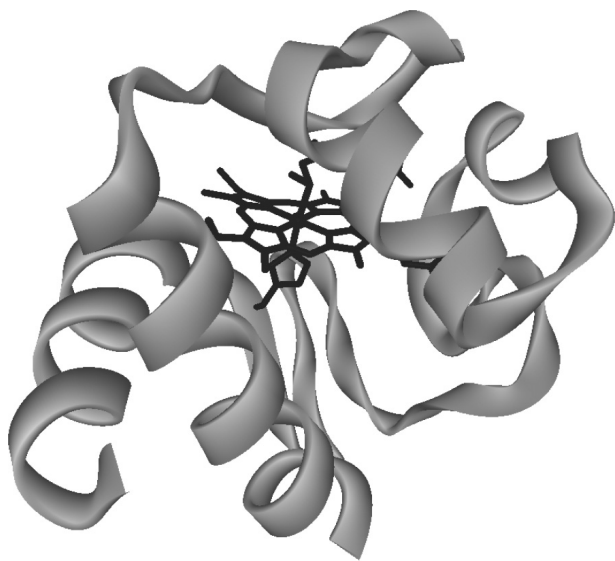


**Figure 2** Ribbon representation of the peptide backbone in horse heart cytochrome *c*. The heme and its axial ligands are shown in black

for electron exchange between Fe(II)- and Fe(III)-cytochrome *c* is 0.8(1) eV.

#### 3.2.2 Azurin

The flash-quench method made it possible to examine high-driving-force ET in labeled copper proteins. *P. aeruginosa* azurin (Figure 3) has a Cu(II/I) reduction potential of 0.31 V vs. NHE.<sup>24</sup> Analysis of the driving-force dependence of Cu(I) → M(III) (M = Ru, Os) ET in M(diimine)<sub>2</sub>(im)(His83)-azurin gives a reorganization energy of 0.8 eV.<sup>44</sup> In accord with this finding, the temperature independence (240–300 K) of Cu(I) → Ru(III) ET in Ru(bpy)<sub>2</sub>(im)(His83)-azurin can be described by  $\lambda_{12} = 0.7 \pm 0.1$  eV, although the observed twofold increase in rate constant as the temperature is lowered to 160 K cannot be explained by changes in the exponential term of the semiclassical rate expression.<sup>45</sup> It is more likely

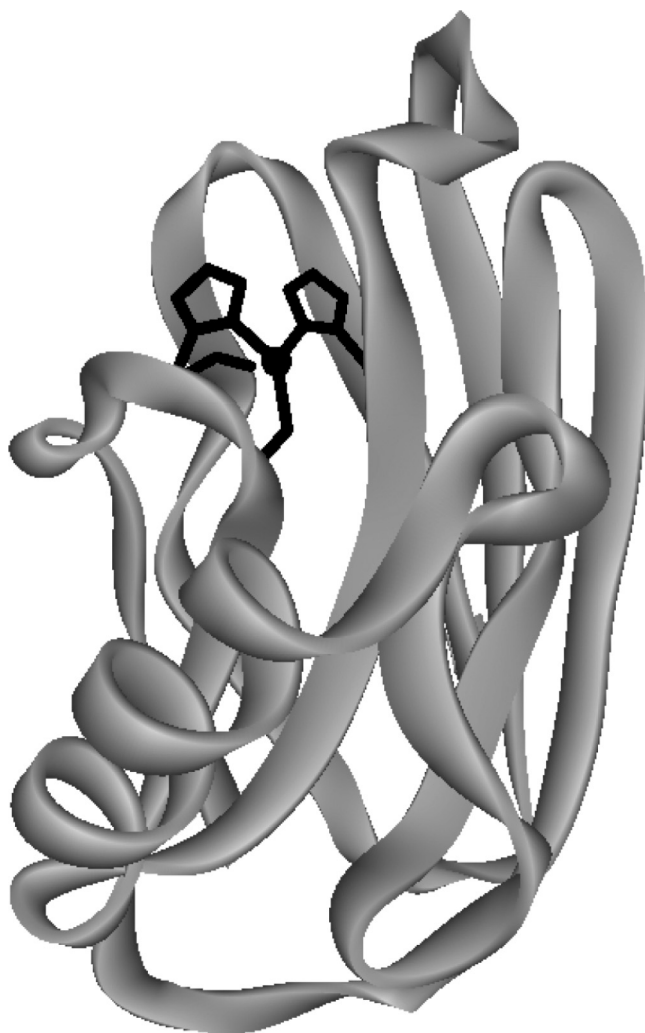


**Figure 3** Ribbon representation of the peptide backbone in *P. aeruginosa* azurin. The Cu cofactor and its ligands are shown in black

that the Ru–Cu electronic coupling increases as the protein is cooled to 170 K.

Rates of Ru(III) and Os(III) reduction by Cu(I) have been measured in single crystals of *P. aeruginosa* M(diimine)<sub>2</sub>(im)(His83)-azurin. In these cases, protein conformation and surface solvation are precisely defined by high-resolution X-ray structure determinations.<sup>46</sup> The time constants for electron tunneling in crystals are roughly the same as those measured in solution, indicating very similar protein structures in the two states. High-resolution structures of the oxidized (1.5 Å) and reduced (1.4 Å) forms of Ru(tpy)(bpy)(im)(His83)-azurin (tpy = 2,2':6,2''-terpyridine; bpy = 2,2'-bipyridine) establish that very small changes in copper coordination accompany reduction.<sup>46</sup> Although Ru(bpy)<sub>2</sub>(im)(His83)-azurin is less solvated in the crystal lattice, the reorganization energy for Cu(I) → Ru(III) electron transfer falls in the same range (0.6–0.8 eV) determined experimentally for the reaction in solution. It is striking that driving forces, reorganization energies, and rates of Cu(I) → M(III) (M = Ru, Os) ET are virtually unchanged when labeled azurins lose one-third of their solvent-accessible surface upon transfer from dilute solutions to crystal lattices with just 40% water. These observations suggest that bulk water plays a minor role in azurin ET reactions; what little solvent reorganization occurs is likely to involve only the ordered waters of hydration.

### 3.3 Tunneling Timetables

Theoretical analyses of coupling pathways in proteins suggest that the efficiency of long-range electron tunneling depends on the secondary structure of the polypeptide between the redox centers.<sup>47</sup> The distance dependence of ET in azurin provides insight into the efficiency of coupling across  $\beta$ -sheet structures.<sup>23</sup> The copper center in azurin is situated at one end of an eight-stranded  $\beta$ -barrel, ligated in a trigonal plane by two imidazoles (His46, His117) and a thiolate (Cys112); in addition, there are weak axial interactions (Met121 thioether sulfur, Gly45 carbonyl oxygen) (Figure 3).<sup>48</sup> The azurin from *P. aeruginosa* has two additional His residues, one of which (His83) reacts readily with Ru-labeling reagents. An H83Q base mutant was prepared and individual mutant His residues were introduced at five locations on  $\beta$ -strands extending from the Cys112 and Met121 ligands (K122H, T124H, T126H, Q107H, M109H). Measurements of Cu(I) → Ru(bpy)<sub>2</sub>(im)(HisX)<sup>3+</sup> ET ( $-\Delta G^\circ = 0.7$  eV) provide a calibration for the distance dependence of ET along  $\beta$ -strands (Figure 4). The driving-force-optimized electron tunneling timetable for azurin reveals an exponential distance dependence, with a decay constant ( $\beta$ ) of 1.1 Å<sup>-1</sup>, and an intercept at close contact ( $r_0 = 3$  Å) of 10<sup>13</sup> s<sup>-1</sup>. This decay constant is quite similar to that found for superexchange-mediated tunneling across saturated alkane bridges ( $\beta \approx 1.0$  Å<sup>-1</sup>),<sup>49</sup> strongly indicating that a similar coupling mechanism is operative in the polypeptide.

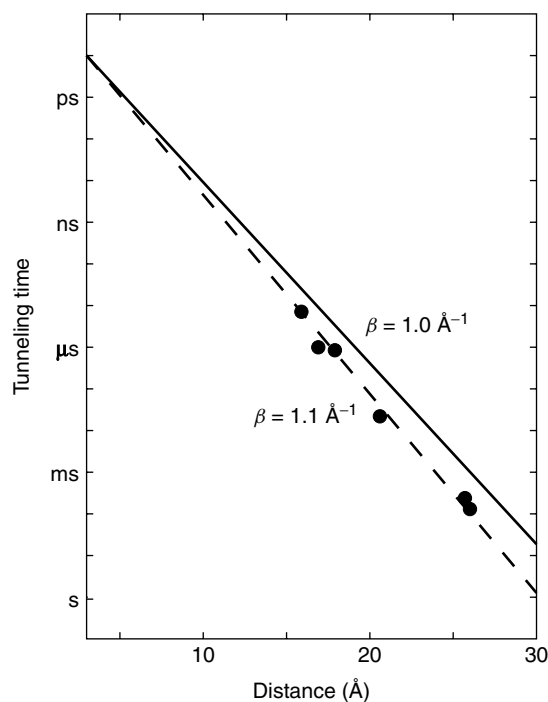


**Figure 4** Distance dependence of driving-force-optimized electron tunneling times in Ru-labeled *P. aeruginosa* azurin. The solid line is the distance decay predicted by the tunneling-pathway model for ET along an ideal  $\beta$ -strand ( $\beta = 1.0$  Å<sup>-1</sup>). The dashed line is the best fit to the data ( $\beta = 1.1$  Å<sup>-1</sup>)<sup>23</sup>

The validity of the azurin tunneling timetable rests on the assumption that Ru-azurin structures are not very different in crystals and aqueous solutions. Measurements of ET kinetics on crystalline samples of labeled azurins directly test this assumption;<sup>46</sup> the rate constants for oxidation of Cu(I) by Ru(III) and Os(III) in solutions and crystals are nearly identical for each donor–acceptor pair. It follows that the crystal structures of reduced and oxidized azurin are the relevant reactant and product states for solution ET.

It is important to distinguish between superexchange-mediated electron tunneling and multistep mechanisms that also can move charge over large molecular distances.<sup>31,32</sup> In tunneling processes, quantum mechanical mixing of localized donor and acceptor states with oxidized (and/or reduced) bridge states couples the reactant and product states, producing an avoided crossing between the free-energy surfaces at the transition state. Neither oxidized nor reduced bridge states are populated in tunneling reactions; ET occurs in a single elementary reaction step. There is a practical upper limit to the separation distance between redox sites; if charges must be transferred farther than this range, then multiple tunneling steps are required. Long-range ET can proceed by either single or multistep tunneling, but each mechanism has distinct energetic and coupling requirements, and can respond quite differently to changes in reaction parameters (e.g.  $T$ ,  $\Delta G^\circ$ ).

The energy gap between the donor/acceptor redox levels and those of oxidized or reduced intermediate states is the primary criterion in determining when multistep tunneling becomes important. In proteins with a single redox cofactor, the opportunities for multistep tunneling are limited. Extreme redox potentials are necessary to oxidize and reduce polypeptide backbones; thus multistep tunneling via backbone states will not contribute to observed ET kinetics under most solution conditions. The side chains of certain amino acids (e.g. Tyr, Trp) have redox potentials that are more accessible than those of the peptide backbone.<sup>50,51</sup> Oxidized Trp and Tyr residues have been characterized spectroscopically in a large number of proteins, although direct evidence for their involvement in multistep tunneling reactions is hard to come by.<sup>52</sup>

The Ru(bpy)<sub>2</sub>(im)(His)<sup>3+/2+</sup> reduction potential ( $E^\circ = 1.0$  V vs. NHE) is not high enough to oxidize Trp or Tyr residues in Ru-azurin; photogenerated holes in Ru(bpy)<sub>2</sub>(im)(HisX)<sup>3+</sup> complexes remain localized on the Ru center. The energy gap between the Ru(III) hole state and oxidized bridge states must therefore be greater than 75 meV ( $3k_B T$  at 295 K). The fact that oxidized bridge states lie at higher energy than the Ru(III) hole does not rule out multistep tunneling; endergonic steps can be compensated by favorable reactions later in a sequence.<sup>32</sup> Endergonic reactions, however, become less effective as the temperature decreases, so that multistep tunneling with highly endergonic steps will exhibit a strong dependence on temperature. The finding that the rate of Cu(I)  $\rightarrow$  Ru(III) ET in Ru(bpy)<sub>2</sub>(im)(HisX)-azurin is nearly independent of temperature between 240 and 300 K, coupled with the observation that decreasing the temperature to 160 K produces a twofold increase in the ET rate, demonstrate that multistep tunneling cannot explain long-range ET in Ru-azurin.<sup>45</sup> Instead, the data shown in Figure 4 provide a calibration standard for superexchange-mediated electron tunneling in proteins.

The rates of high-driving-force ET reactions have been measured for more than 30 Ru(diimine)-labeled metalloproteins.<sup>21,23,24</sup> Only modest corrections are required to scale these rates to driving-force-optimized values, permitting comparisons of ET in different proteins. The results are summarized in the electron tunneling timetable of Figure 5. The reported distances are all metal-to-metal measures; in the case of metal clusters, the closest metal was chosen. Tunneling times range from a few nanoseconds (12.2-Å ET in the high-potential iron-sulfur protein from *C. vinosum*) to 10 milliseconds (26-Å ET in *P. aeruginosa* azurin).

The Ru-protein data points are scattered around the Ru-azurin  $\beta = 1.1 \text{ \AA}^{-1}$  exponential distance decay. More than three-fourths of the Ru-protein ET rates fall in a 1.0 to  $1.3 \text{ \AA}^{-1}$   $\beta$ -value zone. The data in Figure 5 suggest that a canonical distance decay constant will not describe long-range electron tunneling in proteins. Rates at a single distance can differ by as much as a factor of  $10^3$  and D/A distances that differ by as much as 5 Å can produce identical rates. The

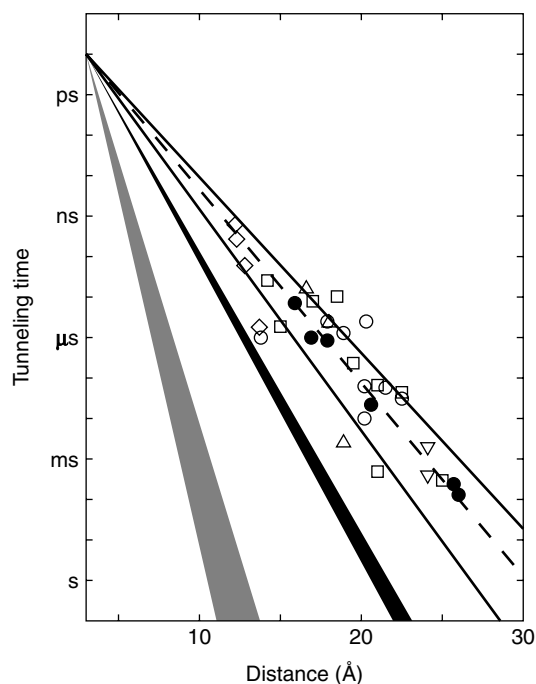


**Figure 5** Tunneling timetable for ET in Ru-modified proteins: azurin (●); cytochrome *c* (○); myoglobin (Δ); cytochrome *b*<sub>562</sub> (□); HiPIP (◇); and Fe:Zn-cytochrome *c* crystals (∇). The solid lines illustrate the tunneling-pathway predictions for coupling along  $\beta$ -strands ( $\beta = 1.0 \text{ \AA}^{-1}$ ) and  $\alpha$ -helices ( $\beta = 1.3 \text{ \AA}^{-1}$ ); the dashed line illustrates a  $1.1 \text{ \AA}^{-1}$  distance decay. Distance decay for electron tunneling through water is shown as a black wedge. Estimated distance dependence for tunneling through vacuum is shown as the grey wedge.<sup>21,23</sup>

absence of a simple exponential distance dependence in the Ru-protein rate data is likely a reflection of the heterogeneity of the coupling medium. The efficiency of the coupling between redox centers is determined by the three-dimensional structure of the intervening polypeptide. While the azurin  $\beta$ -barrel structure supports a relatively uniform distance decay, highly helical proteins (myoglobin, cytochrome *b*<sub>562</sub>)<sup>21,24</sup> exhibit far more heterogeneous behavior. The protein fold is the key determinant of biological ET rates: it establishes the driving force, the reorganization energy, and the electronic coupling.

#### 4 PROTEIN-PROTEIN REACTIONS

In low ionic-strength buffers, many proteins of opposite charge will form relatively tightly bound complexes.<sup>53,54</sup> With the aid of rapid triggering methods, it is possible to measure rates of long-range ET between redox sites in protein-protein complexes.<sup>55,56</sup> In many complexes, there are multiple binding sites and it is not uncommon to find that the ET kinetics often are regulated by the dynamics of conformational

changes in the complex.<sup>54</sup> The usual interpretation is that surface diffusion of the two proteins produces a transient complex with significantly better electronic coupling and faster electron transfer. Consequently, rates depend strongly on solvent viscosity rather than intrinsic ET parameters ( $\Delta G^\circ$ ,  $\lambda$ ,  $r$ ). A further complication associated with studies of protein–protein ET in solution is that binding sites and, hence, locations of redox cofactors, often are unknown. Issues of conformational change and structural ambiguity have been addressed recently with measurements of protein–protein ET kinetics in protein crystals.

#### 4.1 Hemoglobin Hybrids

Kinetics measurements on crystallographically characterized metal-substituted hemoglobin (Hb) hybrids provided some of the earliest insights into interprotein ET rates.<sup>57</sup> Because Hb is a very strongly bound complex of four polypeptide subunits, ET measurements are not complicated by the dynamical problems that plague interpretation of rates in more weakly bound complexes. Replacement of the native Fe center in the  $\beta$ -subunits of Hb with Zn or Mg creates the opportunity for photoinitiated ET reactions. The reacting metal centers in the Hb hybrids are separated by 25 Å so that rates are relatively slow even at high driving forces. The time constant for ET from a triplet-excited ZnPor in the  $\beta$ -subunit to an Fe(III) center in the  $\alpha$ -subunit is about 16 ms. Extensive studies of temperature dependences of hybrid Hb ET rates led to the conclusion that the reorganization energy for these reactions ( $\lambda \sim 1$  eV) is dominated by outer-sphere contributions.<sup>58</sup> Measurements of ET rates in cryogenic glasses suggest that the polypeptide is the primary outer-sphere medium for the reaction and that bulk solvent reorganization does not play an important role in the reaction. Moreover, it was suggested that even at room temperature, the protein medium in Hb acts like a frozen glass. Results from measurements on Ru-azurin crystals also indicate that bulk solvent makes only a minor contribution to protein ET reorganization energies.<sup>46</sup>

#### 4.2 Cytochrome *c*/cytochrome *b*<sub>5</sub> Complexes

The ET reaction between cytochrome *c* and cytochrome *b*<sub>5</sub> has been the subject of experimental and theoretical investigations for more than forty years.<sup>59,60</sup> Modeling both bimolecular and intracomplex ET between these proteins has been an active field of study. The detailed structural model proposed by Salemme in 1976 for the precursor complex of this protein pair stimulated a great deal of experimental work.<sup>61</sup> Careful spectroscopic studies revealed that these oppositely charged proteins form a stable 1:1 complex at low ionic strength.<sup>59</sup>

McLendon and Miller employed a combination of photochemical and pulse-radiolytic methods to probe the driving-force dependence of heme–heme ET in this complex.<sup>53</sup> The ET rates exhibit a near-Gaussian free-energy dependence, in

excellent agreement with a 0.8-eV reorganization energy. The significance of this result is that, although this is a relatively low value of  $\lambda$  for ET between transition metal complexes in aqueous solution, it is by no means optimized. Most biological ET processes release less than 0.3 eV of free energy; with a 0.8-eV reorganization energy, rates will be 1–2 orders of magnitude below their maximum values.

Evidence for more complex ET processes came from studies in which photochemically generated reductants injected electrons into preformed Fe-cytochrome *b*<sub>5</sub>/Fe-cytochrome *c* complexes. In one study, the rate of *b*<sub>5</sub> → *c* ET ( $1.7 \times 10^3$  s<sup>-1</sup>) was reported to depend on viscosity and surface mutations.<sup>62</sup> A later laser-flash photolysis study found a rate-limiting second-order reduction of Fe-cytochrome *b*<sub>5</sub>/Fe-cytochrome *c* complexes and no sign of saturation, suggesting that the intracomplex ET rate was greater than  $10^4$  s<sup>-1</sup>.<sup>59</sup>

Ru-modified cytochrome *b*<sub>5</sub> and photochemical triggering methods were used to examine the kinetics of ET in cytochrome *b*<sub>5</sub>/*c* complexes.<sup>60</sup> Rapid intraprotein reduction (<100 ns) of Fe(III)-cytochrome *b*<sub>5</sub> by excited Ru(bpy)<sub>3</sub><sup>2+</sup> made it possible to probe *b*<sub>5</sub> → *c* ET kinetics. Two concentration-independent ET rates ( $4 \times 10^5$  s<sup>-1</sup>,  $3.4 \times 10^4$  s<sup>-1</sup>) were observed, suggesting that two cytochrome *b*<sub>5</sub>/*c* species are present in solution. Studies of ionic-strength dependences and the effects of mutations suggest that the slower Fe(III)-cytochrome *c* reduction phase may be limited by conformational changes within one of the complexes.<sup>60</sup>

#### 4.3 Cytochrome *c*/cytochrome *c* Peroxidase Complexes

Cytochrome *c* peroxidase (CcP) catalyzes the two-electron reduction of H<sub>2</sub>O<sub>2</sub> by ferrocycytochrome *c*. Hydrogen peroxide reacts rapidly with the resting ferric form of CcP to produce a species referred to as compound I, which contains a ferryl (Fe(IV)O<sup>2+</sup>) heme and a protein radical located on Trp191. The ET reactions involving these physiological redox partners have been studied in great detail.<sup>54</sup> At low ionic strength, acidic CcP and basic cytochrome *c* form a stable complex. A model of a 1:1 complex, based on the crystal structures of the two independent proteins, was proposed by Poulos and Kraut in 1980.<sup>63</sup> Twelve years later, Pelletier and Kraut reported the crystal structure of a 1:1 complex of the two yeast proteins.<sup>64</sup> Interestingly, the complex between yeast CcP and horse cytochrome *c* exhibited a slightly different structure. Analysis of the yeast/yeast complex suggested an electronic coupling pathway from the cytochrome *c* heme to the CcP heme via Trp191. On the basis of these crystallographic results, Pelletier and Kraut argued that CcP and cytochrome *c* form a highly specific 1:1 ET complex.

Hoffman and coworkers have employed metal-substituted CcP and cytochrome *c* to explore the ET kinetics between these two proteins.<sup>54</sup> Results from four-dimensional quenching studies, temperature and ionic-strength dependences, species variations, and electrostatic modeling provide compelling

evidence for two distinct cytochrome *c* binding sites on CcP. The higher affinity binding site is the locus for Trp191 radical reduction by cytochrome *c*. Heme (CcP) reduction by cytochrome *c* can occur from either the high or low affinity binding site but, when exchange between the two is rapid, reduction from the low affinity site dominates.<sup>54</sup> These studies of CcP/cytochrome *c* ET, as well as those of cytochrome *b*<sub>5</sub>/*c*, reveal the considerable mechanistic complexity of protein–protein ET processes.

#### 4.4 Zn-cytochrome *c*/Fe-cytochrome *c* Crystals

Studies of CcP/cytochrome *c* and cytochrome *b*<sub>5</sub>/*c* reactions highlight the difficulty of extracting ET parameters when donors and acceptors are not held at fixed distances and orientations. Crystals containing photoactivatable donors and acceptors at specific lattice sites are ideal media for investigating tunneling between proteins. In crystal lattices of tuna cytochrome *c*, chains of cytochrome *c* molecules form helices with a 24.1-Å separation between neighboring metal centers.<sup>65</sup> All other metal–metal distances in the lattice are greater than 30 Å. Thus, the heme groups can be treated as ordered in a one-dimensional chain, separated by identical protein and solvent media. By doping Zn-cytochrome *c* into this lattice, interprotein ET was probed using laser-flash transient spectroscopy. ET from the triplet-excited Zn-porphyrin to a neighboring Fe(III)-cytochrome *c* proceeded with a rate constant of  $4(1) \times 10^2 \text{ s}^{-1}$ ; the rate of charge recombination was about four times faster ( $2.0(5) \times 10^3 \text{ s}^{-1}$ ).<sup>65</sup>

Rapid relay of electrons involving at least one soluble redox enzyme requires the formation of short-lived, weakly bound protein–protein complexes. The recognition sites between proteins in such complexes tend to be smaller ( $<1200 \text{ Å}^2$ ) and include more water molecules than the interfaces between subunits in oligomeric proteins. The interprotein interactions in crystals of tuna cytochrome *c* involve relatively few contacts: 760 Å<sup>2</sup> of surface area is buried in an interface with 31 van der Waals contacts ( $3.2 \leq d \leq 3.9 \text{ Å}$ ) and 16 water molecules (3 of which form bridging hydrogen bonds across the interface) but only one direct hydrogen bond bridging the two proteins. Indeed, the cytochrome *c*–cytochrome *c* interface is reminiscent of that between the natural redox partners, cytochrome *c* and cytochrome *c* peroxidase (770 Å<sup>2</sup>),<sup>64</sup> and may be typical of the interaction zones for soluble redox proteins. The Zn–Fe separation in doped tuna cytochrome *c* crystals is similar to that in Zn–Fe–hemoglobin hybrids (24.7 Å, T-state), although the tetrameric heme protein has many more contacts between subunits and a greater atom density at the interface. Nevertheless,  $^* \text{ZnPor} \rightarrow \text{Fe(III)}$  and  $\text{Fe(II)} \rightarrow \text{ZnPor}^{+\bullet}$  ET rates in Hb hybrids<sup>57</sup> and Zn-doped tuna cytochrome *c* crystal are quite similar and fall well within the range that has been established in studies of Ru-modified proteins.<sup>21,23,24</sup> The protein crystal ET data demonstrate that small interaction zones of low density are quite effective in mediating interprotein redox reactions.

## 5 PHOTOSYNTHESIS AND RESPIRATION

### 5.1 Photosynthetic Reaction Centers

Bacterial photosynthetic reaction centers (PRC) have been among the most actively studied ET proteins since DeVault and Chance first measured *C. vinosum* tunneling rates in the early 1960s.<sup>66,67</sup> In many cases, measurements of ET kinetics preceded determination of the three-dimensional structure of the membrane-bound protein assembly. It was not until the X-ray crystal-structure determinations of the *Rhodospseudomonas (Rps.) viridus*<sup>68</sup> and *Rhodobacter (Rb.) sphaeroides*<sup>69</sup> PRCs that distances could be assigned to specific rate constants. The recent crystal structures of photosystems I<sup>70,71</sup> and II<sup>72,73</sup> from cyanobacteria promise to clarify critical aspects of the ET mechanisms in oxygenic PRC.<sup>74,75</sup>

Photosynthetic reaction centers are ideal substrates for investigations of long-range electron transfer.<sup>76–78</sup> Charge separation in anoxygenic bacterial PRCs arises from a series of highly optimized ET processes (Figure 6). The primary photochemical event involves 2-ps ET over 17.8 Å from an electronically excited chlorophyll special pair ( $^*(\text{Bchl})_2$ ) to a pheophytin (Bphe) acceptor.<sup>79</sup> The rate of this reaction increases by about a factor of two as the temperature is lowered from 295 to 4 K. The absence of thermal activation indicates that the reorganization energy for  $^*(\text{Bchl})_2 \rightarrow \text{Bphe}$  ET must be close to the driving force (0.2 eV). The reduced pheophytin delivers an electron to a quinone (Q<sub>A</sub>) 14.5 Å away in 100 ps. This productive reaction is 500 times faster than charge recombination with the hole in the bacteriochlorophyll special pair ( $(\text{Bchl})_2^{\bullet+}$ ). In 100 ps, approximately half of the 1.3 eV excitation

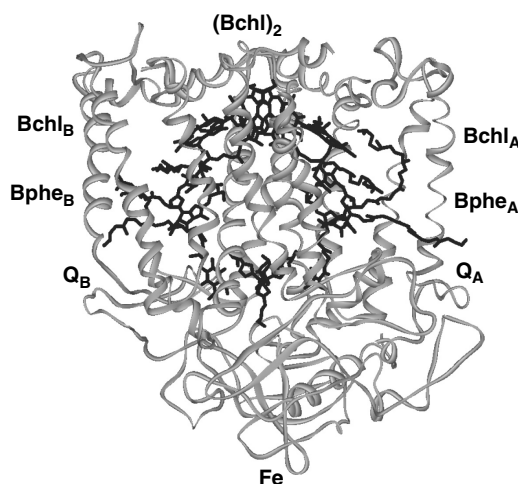


**Figure 6** Model of the X-ray crystal structure of the photosynthetic reaction center from *Rb. sphaeroides*.<sup>69</sup> The bacteriochlorophyll special pair ( $(\text{Bchl})_2$ ), accessory bacteriochlorophylls (Bchl), bacteropheophytins (Bphe), quinones (Q), and iron complex (Fe) are shown in black. Electron transfer proceeds primarily along the A branch

energy of  $^*(\text{Bchl})_2$  has been used to produce a 28.7 Å charge separation.<sup>80</sup> The charge on  $\text{Q}_A$  is subsequently transferred to a second quinone ( $\text{Q}_B$ ) in a proton-coupled ET step.<sup>81,82</sup>

The hole in the bacteriochlorophyll special pair is filled by electron transfer from a cytochrome. In *Rps. viridis*, the cytochrome donor is tightly bound to the PRC at the membrane surface. This subunit contains four hemes in a nearly linear array oriented perpendicular to the membrane.<sup>68</sup> The reduction potentials of the hemes alternate from high ( $\geq 250$  mV vs. NHE) to low ( $\leq 50$  mV) as the distance from  $(\text{Bchl})_2$  increases.<sup>83</sup> The heme closest to the special pair, cytochrome  $c_{559}$ , has the highest potential and fills the  $(\text{Bchl})_2^{\bullet+}$  hole in about  $\sim 200$  ns.<sup>84</sup> The next well-characterized process is ET from cytochrome  $c_{556}$  to cytochrome  $c_{559}$  in  $\sim 2$   $\mu\text{s}$  over a distance of 27.9 Å.<sup>84</sup>

In *Rb. sphaeroides*,  $(\text{Bchl})_2^{\bullet+}$  is reduced by a soluble single heme protein, cytochrome  $c_2$ . Several *Rb. sphaeroides* PRC mutants with altered  $(\text{Bchl})_2^{\bullet+/0}$  potentials have been prepared. In all,  $E^\circ((\text{Bchl})_2^{\bullet+/0})$  values range from a low of 0.410 V to a high of 0.765 V vs. NHE (the wild-type value is 0.505 V).<sup>85</sup> A driving-force study of  $\text{Fe(II)} \rightarrow (\text{Bchl})_2^{\bullet+}$  ET in cytochrome  $c_2$ /PRC complexes gave  $\lambda = 0.5$  eV.<sup>86</sup> Global analysis of temperature and driving-force dependences of these ET rates indicated that  $\lambda = 0.96 \pm 0.07$  eV, and  $H_{AB}$  values were not constant for all of the mutants.<sup>87</sup> The kinetics of ET from cytochrome  $c_2$  to  $(\text{Bchl})_2^{\bullet+}$  in the PRC from *Rb. sphaeroides* have been measured in structurally characterized crystals.<sup>88</sup> The rate ( $1.1 \times 10^6 \text{ s}^{-1}$ ), driving force (0.16 eV), and donor–acceptor distance (21.2 Å) are quite similar to those for ET from cytochrome  $c_{559}$  to  $(\text{Bchl})_2^{\bullet+}$  in *Rps. viridis*.

Photosynthesis works because charge separation is more efficient than energy-wasting charge recombination. By blocking appropriate steps in the charge-separation sequence, it has been possible to determine the rates of PRC charge-recombination reactions. The near-linear arrangement of redox cofactors forms a redox potential gradient that favors short-range charge-separation reactions. In all cases, charge recombinations are many orders of magnitude slower than competing charge-separation reactions.<sup>80</sup>

Many of the PRC ET reactions exhibit only modest variations with temperature. The rate of the primary photochemical event increases at cryogenic temperature.<sup>79</sup> Several other reaction rates decrease by only small factors when temperatures are lowered.<sup>87</sup> For charge separation, this behavior can be attributed to driving-force-optimized reactions.

## 5.2 Cytochrome *c* Oxidase

In the terminal reaction of the respiratory chain, membrane-bound cytochrome *c* oxidase (CcO) receives electrons from soluble cytochrome *c* and passes them on to  $\text{O}_2$ .<sup>1</sup> CcO is a multisubunit membrane-bound enzyme with four redox cofactors ( $\text{Cu}_A$ , cytochrome *a*, cytochrome  $a_3$ ,  $\text{Cu}_B$ ). The

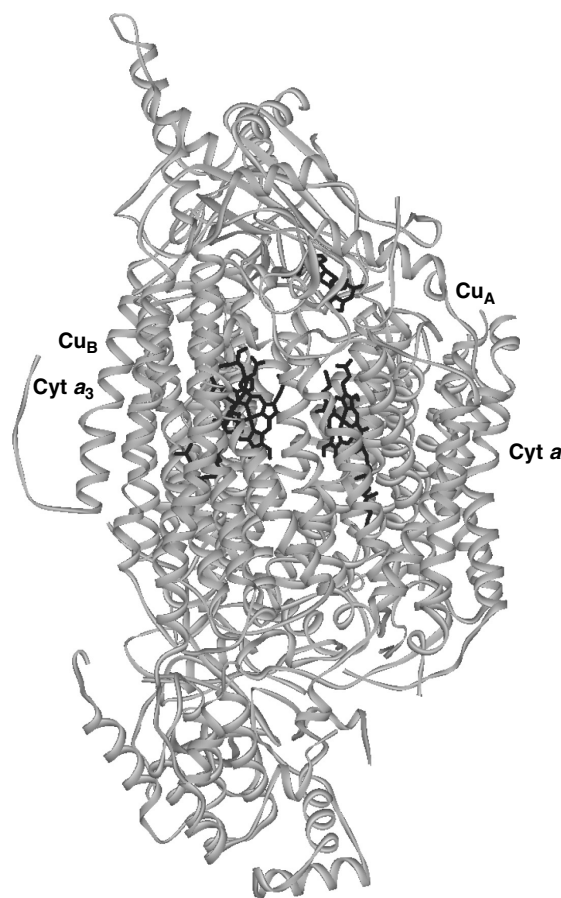


**Figure 7** Model of the X-ray crystal structure of the bovine cytochrome *c* oxidase.<sup>90,91</sup> The dimeric  $\text{Cu}_A$  site, cytochromes *a* and  $a_3$ , and the  $\text{Cu}_B$  center are shown in black. Electrons enter the enzyme through  $\text{Cu}_A$  and oxygen is activated at the cytochrome  $a_3/\text{Cu}_B$  active site

locations of these metal complexes in CcO were revealed in the 1990s by the X-ray crystal structures of bacterial<sup>89</sup> and bovine enzymes (Figure 7).<sup>90,91</sup> The ET reactions of CcO have been the subjects of extensive investigation.<sup>92,93</sup>  $\text{Cu}_A$ , a binuclear Cu site with bridging S(Cys) atoms, is the primary electron acceptor from soluble cytochrome *c*.<sup>94</sup> Studies with Ru-modified cytochrome *c* reveal rapid ( $6 \times 10^4 \text{ s}^{-1}$ )<sup>95</sup> electron injection from Fe(II) into  $\text{Cu}_A$  at low driving force ( $\Delta G^\circ = -0.03$  eV).<sup>96</sup> Modeling suggests that cytochrome *c* binds to the bovine enzyme at an acidic patch on subunit II with an Fe–Cu distance of 17.8 Å.<sup>97</sup> The cytochrome *c* heme in the model is within 3.3 Å of the Trp104 (subunit II) indole ring, a residue that appears from mutagenesis experiments to be critical for rapid cytochrome *c*/ $\text{Cu}_A$  ET. A possible electron tunneling path from this cytochrome *c* binding site through Trp104 to the bridging S(Cys200) ligand on  $\text{Cu}_A$  has been identified.<sup>98</sup>

The 19.6-Å electron transfer from  $\text{Cu}_A$  to cytochrome *a* proceeds rapidly at low driving force ( $1.8 \times 10^4 \text{ s}^{-1}$ ;  $\Delta G^\circ = -0.05$  eV).<sup>95</sup> Multiple electronic coupling pathways have been

proposed for this reaction. One postulated coupling route proceeds from  $\text{Cu}_A$  ligand His204 (subunit II) across one hydrogen bond to Arg438 (subunit I) ( $\text{H204}(\text{N}\epsilon)$ - $\text{R438}(\text{O})$ , 3.36 Å), and another H-bond (2.95 Å) from the Arg438 N-amide to the cytochrome *a* heme-propionate.<sup>1,99-101</sup> A tunneling-currents analysis suggested a slightly different  $\text{Cu}_A$ -cytochrome *a* coupling route through His204.<sup>102</sup> More recent work suggests that, owing to strong Cu-S(Cys) electronic interactions, pathways involving the bridging Cys residues are important for mediating coupling even though they involve more bonds than do routes through His204. Two independent analyses indicated that the sequence Cys200/Ile199/Arg439/heme-propionate (cytochrome *a*) is the dominant coupling route between  $\text{Cu}_A$  and cytochrome *a*.<sup>101,102</sup>

The coupling between cytochrome *a* and cytochrome  $a_3$  has also been examined.<sup>99,102</sup> Nearly equivalent coupling routes between the two hemes involving the axial His residues (His378(cytochrome *a*), His376(cytochrome  $a_3$ )) were identified. One pathway proceeds through the intervening Phe377 residue; the other two involve a hydrogen bond between His378 and Val374. From Ala375, one pathway goes directly to His376 and the other involves a hydrogen bond to Tyr372 (which is hydrogen bonded to His376). A second study identified three major cytochrome *a*/cytochrome  $a_3$  pathways: one is the direct jump from heme *a* to heme  $a_3$ ; one has the aromatic ring of Phe377 as the only intermediate group; and the third involves His378 and the Phe377 aromatic ring. In spite of the similarity in  $\text{Cu}_A$ -cytochrome *a* (19.6 Å) and  $\text{Cu}_A$ -cytochrome  $a_3$  (22.4 Å) distances, pathway analyses do not find important coupling pathways between the  $\text{Cu}_A$  center and cytochrome  $a_3$ .<sup>99,102</sup>

## 6 CONCLUDING REMARKS

It is interesting to compare rates of electron tunneling in CcO and PRC with results from Ru-modified proteins (Figure 8).<sup>80,92</sup> The solid line in the figure corresponds to the average distance dependence of driving-force-optimized ET rates in Ru-proteins ( $\beta = 1.1 \text{ \AA}^{-1}$ ;  $10^{13} \text{ s}^{-1}$  intercept). Most of the observed tunneling rates in CcO and the PRC lie near or above this line, indicating that the natural ET reactions are highly optimized, both in terms of reorganization energy and electronic coupling. Three of the *Rps. viridis* PRC reactions are at least two orders of magnitude faster than would be expected for activationless ET: the initial charge-separation event; ET from cytochrome  $c_{556}$  to cytochrome  $c_{559}$ ; and charge recombination from reduced  $\text{Q}_A$  to cytochrome  $c_{559}$ . These unusually high ET rates may signal the presence of multistep tunneling processes.<sup>79,88,103</sup> It is interesting that neither the  $\text{Q}_A^- \rightarrow (\text{Bchl})_2^{\bullet+}$  nor the  $\text{Q}_A^- \rightarrow$  cytochrome  $c_{559}$  charge-recombination reaction is unusually slow. This contrasts with the  $\text{Bphe}^- \rightarrow (\text{Bchl})_2^{\bullet+}$  reaction, which is  $10^3$  times slower than expected for a driving-force-optimized

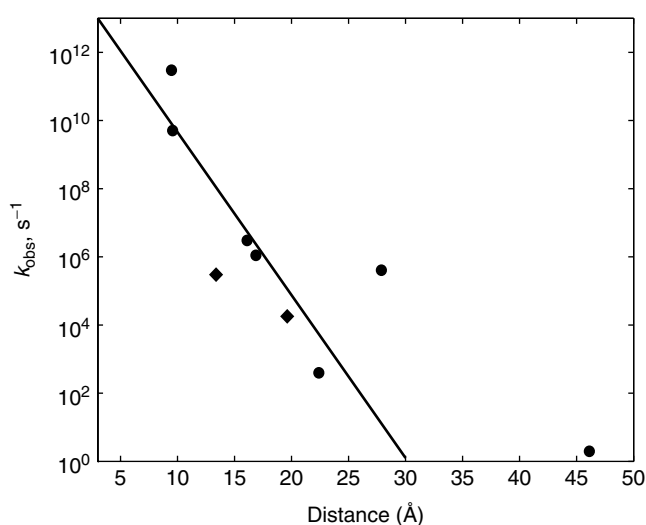


**Figure 8** Distance dependence of observed ET rates in CcO (◆) and the PRC (●).<sup>92,104</sup> The solid line shows the average distance dependence found for driving-force-optimized ET in Ru-modified proteins ( $\beta = 1.1 \text{ \AA}^{-1}$ )

process at the same distance.<sup>80</sup> Inverted driving-force behavior may be responsible for retarding  $\text{Bphe}^- \rightarrow (\text{Bchl})_2^{\bullet+}$  ET, but multistep tunneling may nullify its effects in the longer-range reactions. The rate of ET from  $\text{Cu}_A$  to cytochrome *a* in CcO is close to that expected for an optimized reaction, yet the reaction driving force is just 50 meV. Clearly, both reorganization energies and electronic coupling pathways in CcO have been finely tuned to achieve a high level of electron transport efficiency.

## 7 RELATED ARTICLES

Copper Proteins with Type 1 Sites; Cytochrome Oxidase; Electron Transfer in Coordination Compounds; Electron Transfer Reactions: Theory; Iron: Heme Proteins & Electron Transport; Iron: Heme Proteins, Peroxidases, Catalases & Catalase-peroxidases; Photosynthesis.

## 8 REFERENCES

1. B. E. Ramirez, B. G. Malmström, J. R. Winkler, and H. B. Gray, *Proc. Natl. Acad. Sci. U.S.A.*, 1995, **92**, 11949.
2. P. Brzezinski and G. Larsson, *Biochim. Biophys. Acta Bioenerg.*, 2003, **1605**, 1.
3. B. Giese, *Curr. Opin. Chem. Biol.*, 2002, **6**, 612.
4. M. E. Núñez and J. K. Barton, *Curr. Opin. Chem. Biol.*, 2002, **4**, 199.

5. F. D. Lewis, in 'Electron and Charge Transport Processes in DNA', eds. H. B. Gray and J. R. Winkler, Weinheim, Germany, 2001.
6. N. M. Jackson and M. G. Hill, *Curr. Opin. Chem. Biol.*, 2001, **5**, 209.
7. R. A. Marcus and N. Sutin, *Biochim. Biophys. Acta*, 1985, **811**, 265.
8. R. A. Marcus, *Angew. Chem., Int. Ed. Eng.*, 1993, **32**, 1111.
9. R. A. Marcus, *Adv. Chem. Phys.*, 1999, **106**, 1.
10. H. B. Gray, B. G. Malmström, and R. J. P. Williams, *J. Biol. Inorg. Chem.*, 2000, **5**, 551.
11. C. N. Schutz and A. Warshel, *Proteins: Struct., Funct., Genet.*, 2001, **44**, 400.
12. P. J. Stephens, D. R. Jollie, and A. Warshel, *Chem. Rev.*, 1996, **96**, 2491.
13. F. A. Armstrong and G. S. Wilson, *Electrochim. Acta*, 2000, **45**, 2623.
14. G. R. Moore and G. W. Pettigrew, 'Cytochromes *c*: Evolutionary, Structural, and Physicochemical Aspects', Springer-Verlag, 1990.
15. R. A. Scott and A. G. Mauk, in 'Cytochrome *c* – A Multidisciplinary Approach', University Science Books, Sausalito, CA, 1996.
16. E. L. Raven and A. G. Mauk, *Adv. Inorg. Chem.*, 2001, **51**, 1.
17. F. A. Tezcan, J. R. Winkler, and H. B. Gray, *J. Am. Chem. Soc.*, 1998, **120**, 13383.
18. J. R. Telford, P. Wittung-Stafshede, H. B. Gray, and J. R. Winkler, *Acc. Chem. Res.*, 1998, **31**, 755.
19. P. Wittung-Stafshede, *Acc. Chem. Res.*, 2002, **35**, 201.
20. T. Simonson, *Rep. Prog. Phys.*, 2003, **66**, 737.
21. H. B. Gray and J. R. Winkler, *Q. Rev. Biophys.*, 2003, **36**, 341.
22. M. Bixon and J. Jortner, *Adv. Chem. Phys.*, 1999, **106**, 35.
23. H. B. Gray and J. R. Winkler, *Annu. Rev. Biochem.*, 1996, **65**, 537.
24. J. R. Winkler, A. Di Bilio, N. A. Farrow, J. H. Richards, and H. B. Gray, *Pure Appl. Chem.*, 1999, **71**, 1753.
25. J. J. Hopfield, *Proc. Natl. Acad. Sci. U.S.A.*, 1974, **71**, 3640.
26. A. Ponce, H. B. Gray, and J. R. Winkler, *J. Am. Chem. Soc.*, 2000, **122**, 8187.
27. K. V. Mikkelsen and M. A. Ratner, *Chem. Rev.*, 1978, **87**, 113.
28. H. M. McConnell, *J. Chem. Phys.*, 1961, **35**, 508.
29. A. A. Stuchebrukhov, *Adv. Chem. Phys.*, 2001, **118**, 1.
30. J. N. Onuchic, D. N. Beratan, J. R. Winkler, and H. B. Gray, *Annu. Rev. Biophys. Biomol. Struct.*, 1992, **21**, 349.
31. M. Bixon and J. Jortner, *J. Chem. Phys.*, 1997, **107**, 5154.
32. C. C. Page, C. C. Moser, and P. L. Dutton, *Curr. Opin. Chem. Biol.*, 2003, **7**, 551.
33. W. B. Curry, M. D. Grabe, I. V. Kurnikov, S. S. Skourtis, D. N. Beratan, J. J. Regan, A. J. A. Aquino, P. Beroza, and J. N. Onuchic, *J. Bioenerg. Biomembr.*, 1995, **27**, 285.
34. J. J. Regan and J. N. Onuchic, *Adv. Chem. Phys.*, 1999, **107**, 497.
35. I. A. Balabin and J. N. Onuchic, *J. Phys. Chem. B*, 1998, **102**, 7497.
36. S. S. Skourtis and D. N. Beratan, *J. Biol. Inorg. Chem.*, 1997, **2**, 378.
37. K. Kumar, I. V. Kurnikov, D. N. Beratan, D. H. Waldeck, and M. B. Zimmt, *J. Phys. Chem. A*, 1998, **102**, 5529.
38. A. A. Stuchebrukhov, *J. Chem. Phys.*, 1996, **105**, 10819.
39. F. Millett and B. Durham, *Biochemistry*, 2002, **41**, 11315.
40. K. M. Yocom, J. B. Shelton, J. R. Shelton, W. E. Schroeder, G. Worosila, S. S. Isied, E. Bordignon, and H. B. Gray, *Proc. Natl. Acad. Sci. U.S.A.*, 1982, **79**, 7052.
41. J. R. Winkler, D. G. Nocera, K. M. Yocom, E. Bordignon, and H. B. Gray, *J. Am. Chem. Soc.*, 1982, **104**, 5798.
42. J. R. Winkler and H. B. Gray, *Chem. Rev.*, 1992, **92**, 369.
43. I.-J. Chang, H. B. Gray, and J. R. Winkler, *J. Am. Chem. Soc.*, 1991, **113**, 7056.
44. A. J. Di Bilio, M. G. Hill, N. Bonander, B. G. Karlsson, R. M. Villahermosa, B. G. Malmström, J. R. Winkler, and H. B. Gray, *J. Am. Chem. Soc.*, 1997, **119**, 9921.
45. L. K. Skov, T. Pascher, J. R. Winkler, and H. B. Gray, *J. Am. Chem. Soc.*, 1998, **120**, 1102.
46. B. R. Crane, A. J. Di Bilio, J. R. Winkler, and H. B. Gray, *J. Am. Chem. Soc.*, 2001, **123**, 11623.
47. D. N. Beratan, J. N. Betts, and J. N. Onuchic, *Science*, 1991, **252**, 1285.
48. E. T. Adman, *Adv. Protein Chem.*, 1991, **42**, 145.
49. J. F. Smalley, H. O. Finklea, C. E. D. Chidsey, M. R. Linford, S. E. Creager, J. P. Ferraris, K. Chalfant, T. Zawodzinski, S. W. Feldberg, and M. D. Newton, *J. Am. Chem. Soc.*, 2003, **125**, 2004.
50. J. Stubbe and W. A. van der Donk, *Chem. Rev.*, 1998, **98**, 705.
51. J. Stubbe, D. G. Nocera, C. S. Yee, and M. C. Y. Chang, *Chem. Rev.*, 2003, **103**, 2167.
52. M. C. Y. Chang, C. S. Yee, J. Stubbe, and D. G. Nocera, *Proc. Natl. Acad. Sci. U.S.A.*, 2004, **101**, 6882.
53. G. McLendon and R. Hake, *Chem. Rev.*, 1992, **92**, 481.
54. J. M. Nocek, J. S. Zhou, S. DeForest, S. Priyadarshy, D. N. Beratan, J. N. Onuchic, and B. M. Hoffman, *Chem. Rev.*, 1996, **96**, 2459.
55. V. L. Davidson, *Acc. Chem. Res.*, 2000, **33**, 87.
56. G. Tollin, *J. Bioenerg. Biomembr.*, 1995, **27**, 303.
57. B. M. Hoffman, M. J. Natan, J. M. Nocek, and S. A. Wallin, *Struct. Bonding*, 1991, **75**, 85.
58. L. A. Dick, I. Malfant, D. Kuila, S. Nebolsky, J. M. Nocek, B. M. Hoffman, and M. A. Ratner, *J. Am. Chem. Soc.*, 1998, **120**, 11401.

59. A. G. Mauk, M. R. Mauk, G. R. Moore, and S. H. Northrup, *J. Bioenerg. Biomembr.*, 1995, **27**, 311.
60. B. Durham, J. L. Fairris, M. McLean, F. Millett, J. R. Scott, S. G. Sligar, and A. Willie, *J. Bioenerg. Biomembr.*, 1995, **27**, 331.
61. F. R. Salemme, *J. Mol. Biol.*, 1976, **102**, 563.
62. L. Qin, K. K. Rodgers, and S. G. Sligar, *Mol. Cryst. Liq. Cryst.*, 1991, **194**, 311.
63. T. L. Poulos and J. Kraut, *J. Biol. Chem.*, 1980, **255**, 10322.
64. H. Pelletier and J. Kraut, *Science*, 1992, **258**, 1748.
65. F. A. Tezcan, B. R. Crane, J. R. Winkler, and H. B. Gray, *Proc. Natl. Acad. Sci. U.S.A.*, 2001, **98**, 5002.
66. D. De Vault and B. Chance, *Biophys. J.*, 1966, **6**, 825.
67. D. De Vault, J. H. Parkes, and B. Chance, *Nature*, 1967, **215**, 642.
68. J. Deisenhofer, O. Epp, I. Sinning, and H. Michel, *J. Mol. Biol.*, 1995, **246**, 429.
69. H. Komiya, T. O. Yeates, D. C. Rees, J. P. Allen, and G. Feher, *Proc. Natl. Acad. Sci. U.S.A.*, 1988, **85**, 9012.
70. P. Jordan, P. Fromme, H. T. Witt, O. Klukas, W. Saenger, and N. Krauß, *Nature*, 2001, **411**.
71. P. Fromme, P. Jordan, and N. Krauß, *Biochim. Biophys. Acta*, 2001, **1507**, 5.
72. A. Zouni, H. T. Witt, J. Kern, N. Krauß, W. Saenger, and P. Orth, *Nature*, 2001, **409**, 739.
73. N. Kamiya and J. R. Shen, *Proc. Natl. Acad. Sci. U.S.A.*, 2003, **100**, 98.
74. N. Krauß, *Curr. Opin. Chem. Biol.*, 2003, **7**, 540.
75. J. H. A. Nugent, *Eur. J. Biochem.*, 1996, **237**, 519.
76. Govindjee, J. T. Beatty, and H. Gest, *Photosynth. Res.*, 2003, **76**, 1.
77. Govindjee and H. Gest, *Photosynth. Res.*, 2002, **73**, 1.
78. K. Mobius, *Chem. Soc. Rev.*, 2000, **29**, 129.
79. C. Kirmaier and D. Holten, *Photosynth. Res.*, 1987, **13**, 225.
80. S. Franzen, R. F. Goldstein, and S. G. Boxer, *J. Phys. Chem.*, 1993, **97**, 3040.
81. M. Y. Okamura, M. L. Paddock, M. S. Graige, and G. Feher, *Biochim. Biophys. Acta Bioenerg.*, 2000, **1458**, 148.
82. R. I. Cukier and D. G. Nocera, *Annu. Rev. Phys. Chem.*, 1998, **49**, 337.
83. F. Baymann and F. Rappaport, *Biochemistry*, 1998, **37**, 15320.
84. J. M. Ortega and P. Mathis, *Biochemistry*, 1993, **32**, 1141.
85. X. Lin, H. A. Murchison, V. Nagarajan, W. W. Parson, J. P. Allen, and J. C. Williams, *Proc. Natl. Acad. Sci. U.S.A.*, 1994, **91**, 10265.
86. X. Lin, J. C. Williams, J. P. Allen, and P. Mathis, *Biochemistry*, 1994, **33**, 13517.
87. G. Venturoli, F. Drepper, J. C. Williams, J. P. Allen, X. Lin, and P. Mathis, *Biophys. J.*, 1998, **74**, 3226.
88. H. L. Axelrod, E. C. Abresch, M. Y. Okamura, A. P. Yeh, D. C. Rees, and G. Feher, *J. Mol. Biol.*, 2002, **319**, 501.
89. S. Iwata, C. Ostermeier, B. Ludwig, and H. Michel, *Nature*, 1995, **376**, 660.
90. T. Tsukihara, H. Aoyama, E. Yamashita, T. Tomizaki, H. Yamaguchi, K. Shinzawa-Itoh, R. Nakashima, R. Yaono, and S. Yoshikawa, *Science*, 1995, **269**, 1071.
91. S. Yoshikawa, K. Shinzawa-Itoh, R. Nakashima, R. Yaono, E. Yamashita, N. Inoue, M. Yao, J. M. Fei, C. P. Libeu, T. Mizushima, H. Yamaguchi, T. Tomizaki, and T. Tsukihara, *Science*, 1998, **280**, 1723.
92. J. R. Winkler, B. G. Malmström, and H. B. Gray, *Biophys. Chem.*, 1995, **54**, 199.
93. Ó. Einarsdóttir and I. Szundi, *Biochim. Biophys. Acta Bioenerg.*, 2004, **1655**, 263.
94. H. Beinert, *Eur. J. Biochem.*, 1997, **245**, 521.
95. L. M. Geren, J. R. Beasley, B. R. Fine, A. J. Saunders, S. Hibdon, G. J. Pielak, B. Durham, and F. Millett, *J. Biol. Chem.*, 1995, **270**, 2466.
96. L. P. Pan, S. Hibdon, R.-Q. Liu, B. Durham, and F. Millett, *Biochemistry*, 1993, **32**, 8492.
97. V. A. Roberts and M. E. Pique, *J. Biol. Chem.*, 1999, **274**, 38051.
98. R. K. Szilagy and E. I. Solomon, *Curr. Opin. Chem. Biol.*, 2002, **6**, 250.
99. J. J. Regan, B. E. Ramirez, J. R. Winkler, H. B. Gray, and B. G. Malmström, *J. Bioenerg. Biomembr.*, 1998, **30**, 35.
100. D. R. Gamelin, D. W. Randall, M. T. Hay, R. T. Houser, T. C. Mulder, G. W. Canters, S. de Vries, W. B. Tolman, Y. Lu, and E. I. Solomon, *J. Am. Chem. Soc.*, 1998, **120**, 5246.
101. S. D. George, M. Metz, R. K. Szilagy, H. Wang, S. P. Cramer, Y. Lu, W. B. Tolman, B. Hedman, K. O. Hodgson, and E. I. Solomon, *J. Am. Chem. Soc.*, 2001, **123**, 5757.
102. D. M. Medvedev, I. Daizadeh, and A. A. Stuchebrukhov, *J. Am. Chem. Soc.*, 2000, **122**, 6571.
103. C. C. Page, C. C. Moser, X. Chen, and P. L. Dutton, *Nature*, 1999, **402**, 47.
104. H. B. Gray and W. R. Ellis Jr, in 'Electron Transfer', eds. I. Bertini, H. B. Gray, S. J. Lippard, and J. S. Valentine, University Science Books, Mill Valley, CA, 1994.

### Acknowledgments

I thank Brian S. Leigh for assistance with the graphics. This research is supported by the National Science Foundation and the National Institutes of Health.